ACCOUNTS of chemical research

Article

pubs.acs.org/accounts

Mode-Selective Control of the Crystal Lattice

M. Först,*[,†,‡] R. Mankowsky,[†,‡] and A. Cavalleri*[,†,‡,§]

[†]Max-Planck Institute for the Structure and Dynamics of Matter, Hamburg 22761, Germany

[‡]Center for Free Electron Laser Science, Hamburg 22761, Germany

[§]Department of Physics, Oxford University, Clarendon Laboratory, Oxford OX1 3PU, U.K.

CONSPECTUS: Driving phase changes by selective optical excitation of specific vibrational modes in molecular and condensed phase systems has long been a grand goal for laser science. However, phase control has to date primarily been achieved by using coherent light fields generated by femtosecond pulsed lasers at near-infrared or visible wavelengths.

This field is now being advanced by progress in generating intense femtosecond pulses in the mid-infrared, which can be tuned into resonance with infrared-active crystal lattice modes of a solid. Selective vibrational excitation is particularly interesting in complex oxides with strong electronic correlations, where even subtle modulations of the crystallographic structure can lead to colossal changes of the electronic and magnetic properties.

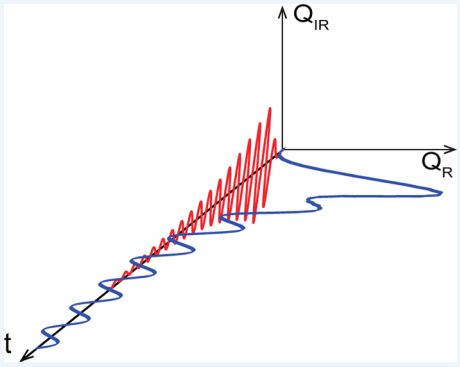

In this Account, we summarize recent efforts to control the collective phase state in solids through mode-selective lattice excitation. The key aspect of the underlying physics is the nonlinear coupling of the resonantly driven phonon to other (Raman-active) modes due to lattice anharmonicities, theoretically discussed as ionic Raman scattering in the 1970s. Such *nonlinear phononic excitation* leads to rectification of a directly excited infrared-active mode and to a net displacement of the crystal along the coordinate of all anharmonically coupled modes. We present the theoretical basis and the experimental demonstration of this phenomenon, using femtosecond optical spectroscopy and ultrafast X-ray diffraction at a free electron laser.

The observed nonlinear lattice dynamics is shown to drive electronic and magnetic phase transitions in many complex oxides, including insulator−metal transitions, charge/orbital order melting and magnetic switching in manganites. Furthermore, we show that the selective vibrational excitation can drive high-T_C cuprates into a transient structure with enhanced superconductivity. The combination of nonlinear phononics with ultrafast crystallography at X-ray free electron lasers may provide new design rules for the development of materials that exhibit these exotic behaviors also at equilibrium.

INTRODUCTION

Coherent optical excitation of infrared-active lattice vibrations in solids is emerging as a new tool to control the crystal structure of solids directly and to drive phase transitions dynamically. Particularly in correlated electronic systems, where the phase state is determined by the interactions between charges, orbitals, spins, and the crystal lattice,[1] these optically driven lattice distortions lead to colossal rearrangements in the electronic and magnetic properties, opening up many opportunities for applications in ultrafast data processing and storage. Especially attractive is the ability to switch the functionality of these solids at high speeds, while minimizing heating and dissipation.

These advances are related to previous work aimed at driving chemical reactions by the coherent control of specific molecular vibrations,[2,3] in what is often referred to as "bond selective chemistry". However, bond selective chemistry has been often severely limited by the large atomic motions needed to break or make chemical bonds. These dynamical distortions inevitably lead to uncontrolled energy transfer to molecular and bath modes, an effect typically referred to as internal vibrational redistribution.[4,5] Hence, the applicability of bond selective control to chemical reactions has so far been limited.

Such limitations are far less important in the solid state. First, due to cooperativity, the unit cell distortions that accompany a phase transition are far smaller than the bond dilations and bond breaking necessary for a chemical reaction. It is not uncommon to observe enormous changes in the macroscopic properties of solids for minute lattice distortions, sometimes of only a few percent of the equilibrium lattice constant. This is especially true for complex materials, in which electronic correlations make the collective properties of the solid a highly nonlinear function of many perturbations. Second, the internal vibrational redistribution is far less pronounced in crystalline solids, where translational invariance limits the density of states of the lattice modes and introduces momentum-conservation constraints for the decay of vibrational energy.

In this Account, we present some recent advances in this area. We first discuss how anharmonic energy flow among different modes is key to atomic structural control. We show how cubic anharmonicities lead to net displacements of the crystal lattice. We then summarize some recent experimental demonstrations for this *nonlinear phononics*, which involve both

Received: October 24, 2014
Published: January 16, 2015

DOI: 10.1021/ar500391x
Acc. Chem. Res. 2015, 48, 380−387

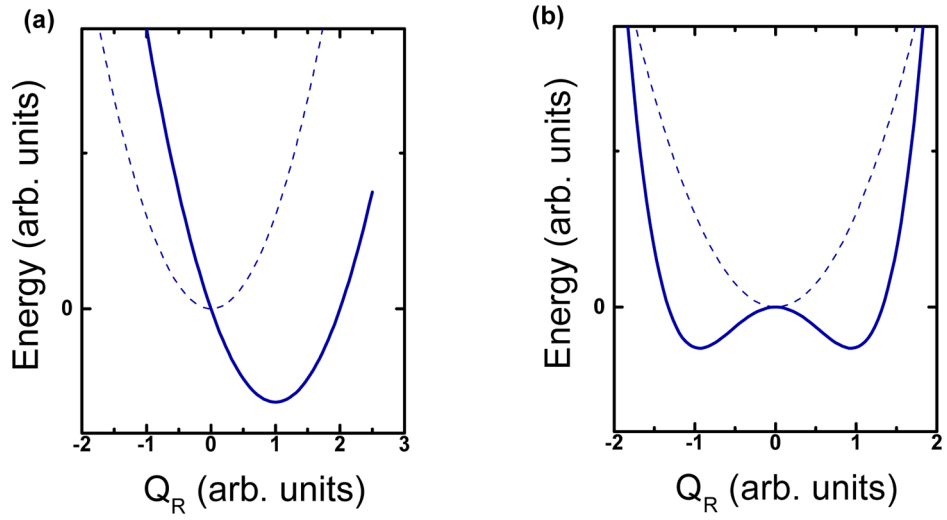

Figure 1. (a) Parabolic energy potential of a Raman-active phonon mode (dashed curve). This potential shifts when a static infrared distortion takes place. For cubic coupling, the potential energy is displaced (solid curve). (b) For quartic coupling, the potential is not shifted but softened (or stiffened). For the case of softening, beyond a certain threshold the potential becomes unstable and can lead to a symmetry breaking transition.

ultrafast X-ray and ultrafast optical probing. We also show how nonlinear control of the crystal lattice can be used to drive phase transitions, hence inducing large cooperative response in a solid. Finally, we discuss how mode-selective nonlinear phononics has been used to enhance superconductivity in the high-T_C cuprates, a phenomenon that is only partially understood.

NONLINEAR PHONONICS

The linear response of a crystal lattice to a light field made resonant with an infrared-active phonon mode is described by the potential energy term $H_{lin} = (1/2)\omega_{IR}^2 Q_{IR}^2$. In this expression, Q_{IR} is the normal coordinate of the mode and ω_{IR} its frequency. When driven by a pulsed field of the type $f(t) = F(t)\sin(\omega_{IR}t)$, for which $F(t)$ is a Gaussian envelope function, the dynamics is described by the equation of motion of a damped harmonic oscillator

$$\ddot{Q}_{IR} + 2\gamma_{IR}\dot{Q}_{IR} + \omega_{IR}{}^2 Q_{IR} = f(t) \quad (1)$$

where ω_{IR} and γ_{IR} are the eigenfrequencies and damping constants of the mode, respectively. Hence, the atoms oscillate about their equilibrium positions along the normal coordinate of the mode and relax over a time scale determined by the duration of the envelope function or by the damping time, $1/\gamma_{IR}$, whichever is longer.

When the strength of the driving electric field increases, anharmonic coupling to other modes with generic coordinate Q_R becomes important. In the limit of cubic coupling, the lattice Hamiltonian can be expressed as $H = H_{lin} + H_{NL}$, with

$$H_{NL} = \frac{1}{2}\omega_R{}^2 Q_R{}^2 - a_{12} Q_{IR} Q_R{}^2 - a_{21} Q_{IR}{}^2 Q_R \quad (2)$$

where a_{ij} are the anharmonic coupling constants. Equation 2 is simplified if we restrict the discussion to centrosymmetric crystals, for which infrared-active phonon modes are of odd parity and Raman-active modes are even. In this case, the first coupling term, $a_{12}Q_{IR}Q_R{}^2$ is always zero and the second term $a_{21}Q_{IR}{}^2Q_R$ is nonzero only if Q_R is of Raman symmetry. For a finite static amplitude Q_{IR}^* of the infrared-active mode, this nonlinear phonon interaction manifests itself in a shift of the energy potential of the Raman mode, as shown in Figure 1a.

The dynamics is described by the two coupled equations of motion

$$\ddot{Q}_{IR} + 2\gamma_{IR}\dot{Q}_{IR} + \omega_{IR}{}^2 Q_{IR} = 2a_{21} Q_{IR} Q_R + f(t) \quad (3)$$

$$\ddot{Q}_R + 2\gamma_R\dot{Q}_R + \omega_R{}^2 Q_R = a_{21} Q_{IR}{}^2 \quad (4)$$

The key feature of cubic coupling is the appearance of a driving force onto one or more anharmonically coupled modes Q_R when Q_{IR} is driven periodically. This driving force is given by the expression $a_{21}Q_{IR}{}^2$ in eq 4.

Due to this force, the atoms not only oscillate along the infrared coordinate Q_{IR} (red curve in Figure 2) but also are simultaneously displaced along the Raman coordinate Q_R (blue curve in Figure 2). This effect is the equivalent of rectification in nonlinear optics. Furthermore, if the period T_R of the Raman mode oscillations is longer than the duration of the infrared pulse, coherent oscillations along Q_R are induced (see blue

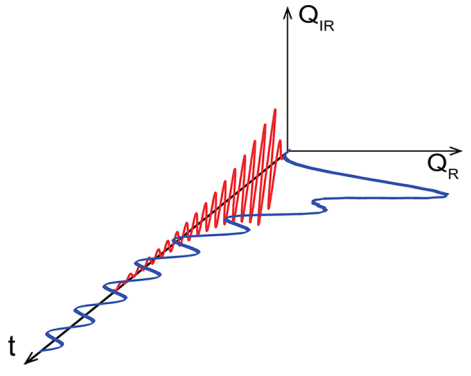

Figure 2. Dynamical response of the two modes in the limit of cubic coupling involves an oscillatory motion of the infrared mode (red) and a directional displacement of Q_R (blue). This displacement is proportional to $Q_{IR}{}^2$ and survives as long as Q_{IR} is coherent. If the optical pulse is shorter than the Raman phonon period, coherent oscillations take place along Q_R, which decay with the dephasing time of the Raman mode.

DOI: 10.1021/ar500391x
Acc. Chem. Res. 2015, 48, 380−387

curve in Figure 2). This physics was already analyzed theoretically[6−8] for the case of incoherent generation of Raman phonons. However, this phenomenon, then termed "ionic Raman scattering", was never observed due to lack of intense optical sources in the mid-infrared. Here, we shall refer to the coherent excitation of lattice modes by nonlinear phononics as stimulated ionic Raman scattering.

These two effects, a displacement and oscillations, are also characteristic of the well-known response of crystal lattices to pulsed excitation in the near-IR or visible.[9−11] However, in that case the lattice displacement and oscillations are driven by electron−phonon coupling and not, as is the case for nonlinear phononics, by lattice anharmonicities. Note also that for the case of nonlinear phononics the excitation is more selective and dissipation is by far reduced due to the low photon energy and the associated strongly reduced number of accessible energy relaxation channels.

Quartic nonlinearities may be expected at large enough field strengths, when terms of the type $a_{22}Q_{IR}^2Q_R^2$ may become sizable. For small static displacements Q_{IR}^*, the quartic coupling is characterized by a broadening of the Q_R energy potential, that is, a softening of this mode. Above a certain threshold, the eigenfrequency becomes imaginary and the energy potential gradually changes from the parabolic to a symmetric double-well shape (see Figure 1b). In turn, the crystal will be distorted into a new structure. Note that in this case the atoms are displaced into one of two possible directions, which would presumably be selected by the instantaneous position and velocity of the atoms. However, this effect is likely to be considerably smaller than the cubic coupling and becomes important only if the latter is forbidden by symmetry. There are virtually no symmetry restrictions for quartic interaction, and coupling to any other phonon mode in a crystal, both infrared and Raman active, is allowed.

EXPERIMENTAL DEMONSTRATION

In the following, we discuss the first experimental observations of nonlinear phononics in the rhombohedrally distorted perovskite $La_{0.7}Sr_{0.3}MnO_3$, a double-exchange ferromagnet with low electrical conductivity ($T_c \approx 350$ K). Many unscreened infrared-active phonon modes are found in this material, with a Mn−O stretching mode of E_u symmetry at 605 cm^{-1} (20 THz).[12] In the experiments discussed here, a resonant mid-infrared pump pulse excited this mode to large amplitude.

Figure 3a displays the time-dependent optical reflectivity changes that follow the excitation of this mode, measured by mid-infrared (15 μm wavelength) pump−near-infrared (800 nm wavelength) probe experiments.[13] Crucially, the ultrafast optical response exhibits clear reflectivity oscillations at 1.2 THz, indicative of the excitation of a Raman mode and corresponding to the frequency of the E_g symmetry mode, involving the rotation of oxygen octahedra around the Mn cations. The symmetry assignment is substantiated by the polarization dependence of the oscillatory signal, which shows a 180° phase shift for two orthogonal probe polarizations, characteristic of E_g symmetry. In addition, the pump wavelength dependent amplitude of the coherent E_g Raman mode oscillations follows the resonance profile of the infrared-active Mn−O stretching vibration, as shown in Figure 3b.

These all-optical measurements clearly identify the frequency and the symmetry of the coherently driven Raman mode. The phase of the oscillations may carry some information on the

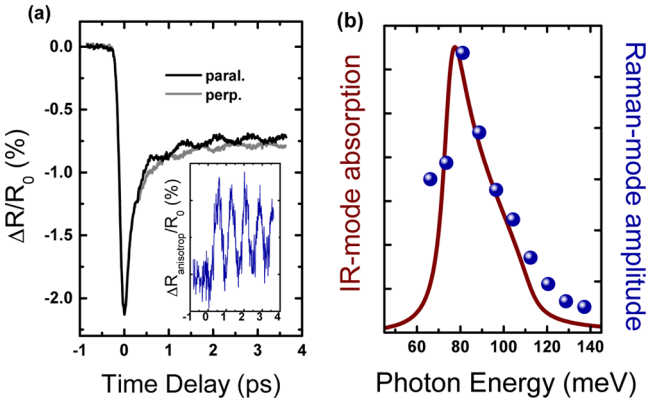

Figure 3. (a) Time-resolved reflectivity changes in a $La_{0.7}Sr_{0.3}MnO_3$ single crystal induced by the resonant excitation of the infrared-active E_u-symmetry Mn−O stretching vibration at 14.3 μm wavelength (87 meV photon energy). The excitation fluence is 2 mJ/cm^2. The 800 nm probe pulses are set to two orthogonal polarizations, and the inset shows the anisotropic lattice-induced signal contributions. (b) Pump photon energy dependent amplitude of the coherent E_g-symmetry Raman phonon shown in panel a.

excitation process;[11,14] however the lattice displacement predicted by the model of nonlinear phonon coupling cannot be directly proven. From the optical probe data shown in Figure 3a, it is not possible to uniquely establish whether the Raman-mode oscillates coherently around the atomic positions of the displaced crystal structure or around those of the unperturbed ground state.

Therefore, the motion of the crystal lattice was studied with a complementary technique by measuring ultrafast X-ray diffraction in combination with ultrafast mid-infrared excitation.[15] In these experiments, the intensity modulation of an X-ray Bragg peak, as resulting from atomic motions along the phonon coordinate, was determined by the ultrafast changes in the X-ray structure factor.[16,17] For the case of the rotational E_g Raman mode, one expects antiphase rotations of the two MnO_6 octahedra of the $La_{0.7}Sr_{0.3}MnO_3$ unit cell,[18,19] as illustrated in Figure 4. Because only motions of the oxygen atoms are

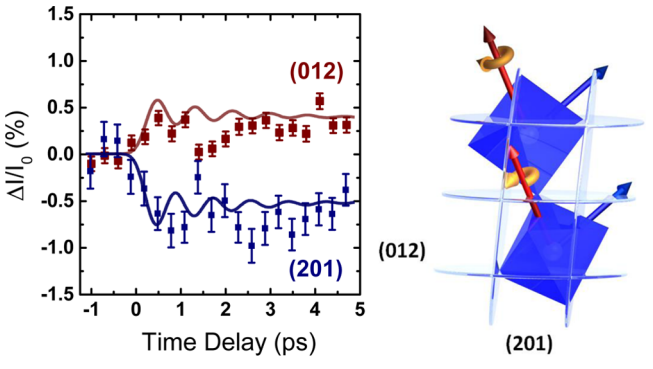

Figure 4. Time-resolved intensity changes of the (012) and the (201) Bragg reflections in $La_{0.7}Sr_{0.3}MnO_3$, induced by the same mid-infrared excitation as the all-optical experiments shown in Figure 3. These Bragg peaks are sensitive to the rotational motions of the MnO_6 octahedra associated with the E_g-symmetry Raman mode (see also illustration on the right-hand side). The solid lines are the intensity changes calculated from the coupled equations of motion and the structure factors of the respective lattice peaks, with the anharmonic coupling constant being the only fitting parameter.

DOI: 10.1021/ar500391x
Acc. Chem. Res. 2015, 48, 380−387

involved, we measured diffraction from the {201} family of reflections, forbidden in the Mn and La/Sr sublattices of rhombohedral $La_{0.7}Sr_{0.3}MnO_3$ and hence exposing the motion of the oxygen atoms. We note here that due to the small scattering of the oxygen atoms this measurement involves a very inefficient Bragg reflection, and it is only possible thanks to the high flux of an X-ray free electron laser.

Figure 4 summarizes the results of femtosecond X-ray diffraction experiments carried out at the Linac Coherent Light Source (LCLS) free electron laser.[20] Here, the transient intensity changes of the (201) and the (012) lattice peaks were measured with 6 keV, 70 fs X-ray pulses.

Two displacive responses were observed in the transient Bragg intensities, with different amplitudes and opposite signs for the different peaks. These curves were fitted by a numerical solution of the coupled equations of motion, eqs 2 and 3, furthermore taking into account the calculated relative intensity changes $(\Delta I/I_0)/Q_R$ for a motion of the oxygen atoms with amplitude Q_R along the coordinate of the Raman mode. Note that the anharmonic coupling constant a_{21} was the only parameter that has been chosen to best fit the calculations to the experiment. These fits indicate that the correct sign and ratio of the two structure factor changes are measured and reveal a rotation of the MnO_6 octahedra of 0.035°. However, the coherent phonon oscillations predicted by the model and observed in the optical probe experiment (see Figure 3) could not be resolved, likely because of the small signal-to-noise ratio in the measurement of these weak reflections.

DRIVING PHASE CHANGES BY NONLINEAR PHONONICS

The atomic motions revealed above for the case of rhombohedral $La_{0.7}Sr_{0.3}MnO_3$, for which the resonant excitation of the Mn−O stretching mode is converted into the rotation of the oxygen octahedra, opens interesting possibilities to control the collective electronic properties of manganites. The rotational motion of the octahedra is in fact particularly important because it controls the Mn−O−Mn bond angles, which themselves strongly affect the electronic and magnetic properties. This effect results from the sign of the exchange interaction, which for a semicovalent bond depends on the spatial overlap of the orbital wave functions along these bonds.

The magnetic and structural properties of manganites can be understood by considering the Goodenough−Kanamori (GK) rules[21] for semicovalent bonds. These rules explain the sign of the exchange interaction between neighboring manganese cations (Mn^{3+} or Mn^{4+}) connected by an oxygen anion (O^{2-}). According to the GK rules, the exchange integral J will always be negative, that is, promote antiferromagnetic alignment, if the semicovalent bond is formed between two half-filled (Mn^{3+}) orbitals or between two empty orbitals (Mn^{4+}). Antiferromagnetic bonding is, as a rule, associated with insulating behavior along the chain, because the hopping is inhibited by Pauli's exclusion principle. However, when the bond is between a half-filled orbital (Mn^{3+}) and an empty orbital (Mn^{4+}), as is the case for doped manganites like $La_{0.7}Sr_{0.3}MnO_3$ or $Pr_{0.7}Ca_{0.3}MnO_3$, either ferromagnetic metallic or antiferromagnetic insulating behavior is possible, as constrained by the onsite Hund interaction. Generally, one finds that for asymmetric Mn^{3+}−O^{2-}−Mn^{4+} bonds, hopping occurs and the magnetic coupling is ferromagnetic as long as the bond is "straight". A "bent" bond, with an angle ≪180° corresponds to an insulating, antiferromagnetic phase.

This complex interplay and phase competition is especially evident in the octahedral manganite $Pr_{0.7}Ca_{0.3}MnO_3$, which is an insulator because of its strongly distorted perovskite structure. However, these properties are unstable against many forms of perturbation.[22−26] Importantly, a metallic phase can be induced by application of static pressure,[27] for which the lattice distortion qualitatively "straightens" the bonds.

Experiments in $Pr_{0.7}Ca_{0.3}MnO_3$ by Rini et al.[28] revealed a prompt increase in conductivity by nearly 5 orders of magnitude after resonant excitation of the Mn−O stretching vibration at ∼17 μm wavelength. Figure 5a shows the transient

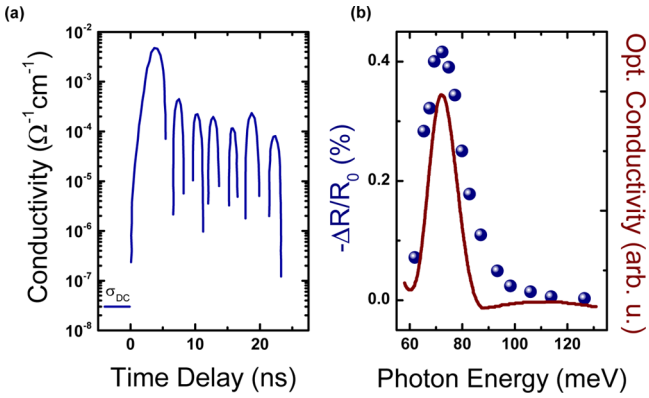

Figure 5. (a) Time-dependent electric conductivity of a $Pr_{0.7}Ca_{0.3}MnO_3$ single crystal following resonant excitation of the Mn−O stretching vibration in the mid-infrared. The DC conductivity, measured at negative time delay, is drastically increased as result of the insulator−metal transition. (b) Photon energy dependence of the strength of the insulator−metal transition, derived from an optical probe experiment. For comparison, we also plot the absorption spectrum convolved with the spectral width of the mid-infrared excitation pulses.

changes in electric transport measured following ∼mJ/cm^2 excitation of a $Pr_{0.7}Ca_{0.3}MnO_3$ single crystal, measured by direct current transport with a fast oscilloscope. The transition from the insulating ground state into the metastable metallic state is evident from the large increase in electrical conductivity within the first 5 ns. Note that the time resolution of this experiment was 4 ns, and the ringing at later time delays results from an artifact resulting from the fast conductivity changes and the imperfect impedance matching to the oscilloscope.

Strikingly, this light-induced phase change follows the same pump wavelength dependence of the nonlinear phonon response discussed above in Figure 3. The strength of the insulator−metal transition in $Pr_{0.7}Ca_{0.3}MnO_3$, measured in an optical probe experiment,[28] clearly follows the resonance of the Mn−O stretching mode in this compound (see Figure 5b).

Density functional theory calculations for the coupling strength between the resonantly driven B_{1u} symmetry Mn−O stretching mode and the Raman modes of parent compound $PrMnO_3$, performed by Subedi et al.,[29] substantiate the interpretation discussed above. The energy potential of a strongly coupled A_g symmetry Raman mode is shown in Figure 6a for fixed amplitude Q_{IR} of the B_{1u} mode. Finite B_{1u} mode amplitude shifts the parabolic potential of the A_g mode to a new minimum position, where the displacement of this mode from the equilibrium increases with larger amplitude of the B_{1u} mode. As shown in Figure 6a, the atomic motions associated with the positive amplitude bring the crystal structure closer to

DOI: 10.1021/ar500391x
Acc. Chem. Res. 2015, 48, 380−387

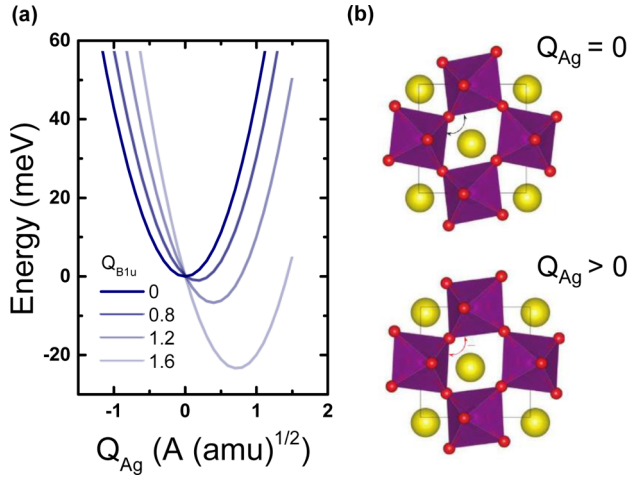

Figure 6. (a) Calculated energy potentials of the A_g Raman mode in $PrMnO_3$ for different static displacements of the infrared-active B_{1u} mode. (b) Atomic positions of the orthorhombically distorted perovskite at equilibrium (top) and for finite positive amplitude Q_{Ag} of the in-plane rotational Raman mode (bottom).

the cubic perovskite, that is, flatten the Mn−O−Mn bonds. According to the nonlinear phononics concept, the excitation of the B_{1u} mode by an intense mid-infrared pulse will displace the crystal lattice along these coordinates. The insulator−metal transition becomes apparent by calculations of the electronic density of states of the manganese 3d orbitals in this compound by dynamical mean field theory, which yield a gap at the Fermi energy for the equilibrium crystal structure and a closing of this gap in the displaced state.[29]

Time-resolved resonant soft X-ray diffraction at the LCLS free electron laser was also used. The ultrafast response of the orbital and magnetic order to vibrational excitation was studied in the related layered manganite $La_{0.5}Sr_{1.5}MnO_4$,[30,31] The reduction of both orders following resonant excitation of the infrared-active in-plane Mn−O stretching mode was observed by measuring the transient intensity changes of certain superlattice reflections for photon energies made resonant with the 640 eV Mn L-edge (see Figure 7a) and hence sensitive to the arrangement of the Mn 3d electrons.[32] This response was understood by considering that according to selection rules, this B_{2u}-symmetry mode can couple nonlinearly to a Raman-active A_g-symmetry Jahn−Teller mode, sketched in Figure 7b. In the equilibrium state, Jahn−Teller distortions lift the degeneracy of the 3d orbitals to lower the energy of the system, concomitantly stabilizing orbital ordering and affecting exchange interactions to also induce magnetic ordering. The displacement of this Jahn−Teller mode was then proposed to relax these distortions, thus melting the ordering of orbitals and spins in the driven state.

We note again that the ultrafast physical pathway of this lattice-driven insulator−metal control in the manganites is different from excitation at infrared or visible wavelengths. In the latter case, the phase transition is triggered by the transfer of charges between different orbitals or adjacent sites, subsequently releasing Jahn−Teller distortions and modifying the exchange interactions.[33−35] Differences in the microscopics of the long-lived product states for the two types of excitations could be unambiguously determined in a time-resolved diffraction experiment that simultaneously discloses the charge order, the orbital order, and the lattice dynamics.[36]

■ ENHANCING SUPERCONDUCTIVITY BY NONLINEAR PHONONICS

The discussion above highlights how nonlinear lattice dynamics can drive an insulator-to-metal transition and magnetic switching in the doped manganites. Similar effects were shown to take place in other highly correlated electron systems such as nickelates[37] and high-T_C cuprates, in which light-induced superconductivity was observed.[38,39]

A striking achievement of nonlinear phononics was recently demonstrated in the high-temperature superconductor $YBa_2Cu_3O_{6+x}$, where direct lattice excitation was shown to enhance coherent transport below T_C and to induce a transient

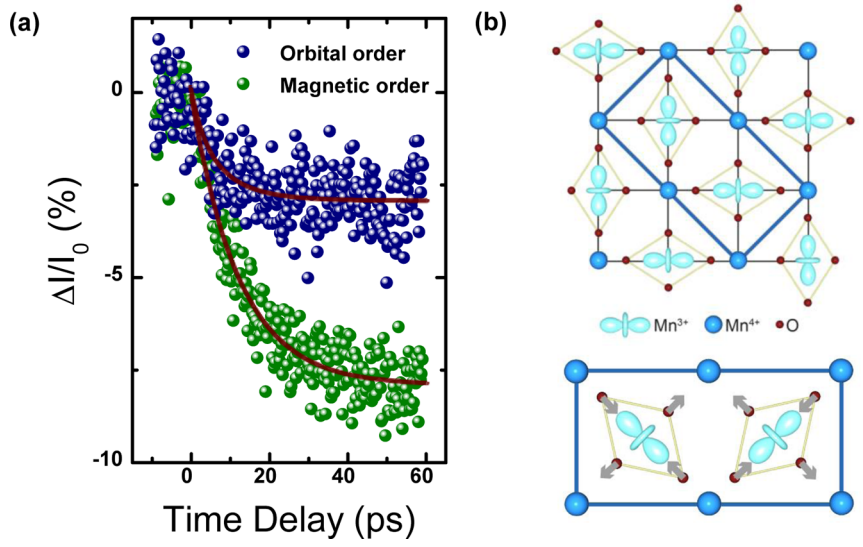

Figure 7. (a) Lattice-driven melting of antiferromagnetic and charge/orbital order in the layered manganite $La_{0.5}Sr_{1.5}MnO_4$, measured via time-resolved resonant soft X-ray diffraction. (b) Sketch of the equilibrium in-plane charge and orbital order, with the orbital ordering unit cell indicated as the thick blue line (top). Displacement of the oxygen atoms associated with the nonlinearly coupled Raman-active A_g symmetry Jahn−Teller mode. The sketched relaxation of the Jahn−Teller distortions drives the order melting.

DOI: 10.1021/ar500391x
Acc. Chem. Res. 2015, 48, 380−387

state with important similarities to the equilibrium superconductor up to room temperature.[40,41]

The equilibrium crystal structure of orthorhombic $YBa_2Cu_3O_{6.5}$ (T_C = 52 K) is schematically shown in Figure 8a. It is composed of bilayers of conducting CuO_2 planes,

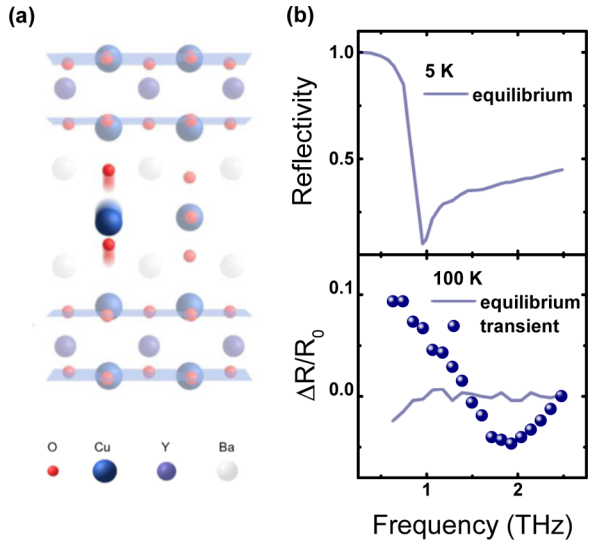

Figure 8. (a) Equilibrium crystal structure of $YBa_2Cu_3O_{6.5}$ and sketch of the B_{1u}-symmetry infrared-active apical oxygen phonon mode. (b) Below-T_C static frequency-dependent terahertz reflectivity polarized along the crystal *c*-axis. The lower panel shows the light-induced reflectivity changes above T_C (100 K, blue dots) at +0.8 ps time delay after excitation with 300 fs pulses at 15 μm wavelength, polarized along the *c*-axis. The light blue solid line shows the same signal at negative time delay.

themselves comprising buckled O−Cu−O bonds, that are separated by an insulating layer containing yttrium atoms and Cu−O chains. The three-dimensional superconducting state below T_C is characterized by coherent transport (Josephson tunneling) of Cooper pairs both between the two 2D-superconducting CuO_2 planes forming a bilayer and between the bilayers. The so-called Josephson plasma mode, which results from supercurrent oscillations between the capacitively coupled bilayers, carries an optical signature of this 3D superconductivity[42] that can be traced in a time-resolved experiment. It is a longitudinal mode with the plasma frequency mainly determined by the density of the Cooper-pair condensate and the distance between the superconducting layers. The Josephson plasma resonance becomes apparent as a characteristic edge in the terahertz reflectivity along the crystallographic *c* axis, as shown for a $YBa_2Cu_3O_{6.5}$ sample at 5 K lattice temperature in the top panel of Figure 8b. For this measurement, single-cycle terahertz pulses were generated by optical rectification in nonlinear optical crystal and measured after reflection from the sample using electro-optic sampling.

Above the critical temperature, the spectrally resolved terahertz reflectivity is flat (Figure 8b, bottom, light blue solid line). Resonant excitation of the infrared-active B_{1u}-symmetry lattice distortion sketched in Figure 8a with 300 fs, 15 μm mid-infrared pulses drives the systems into a nonequilibrium state that again exhibits a Josephson plasma resonance, that is, the optical signature of equilibrium superconductivity below T_C (Figure 8b).

Femtosecond hard X-ray diffraction experiments were carried out at the LCLS free electron laser to reveal the nonlinear lattice dynamics underlying this effect.[43] For symmetry reasons, the resonantly driven B_{1u} phonon mode in $YBa_2Cu_3O_{6.5}$ can only couple to Raman-active phonons of A_g symmetry. Among those 11 modes, four lattice vibrations, all involving a concerted distortion of the apical oxygen atoms toward the CuO_2 plane and an enhanced in-plane Cu−O buckling, were identified by DFT calculations to strongly couple to the specific lattice excitation. Thus, according to the concept of nonlinear phononics, we expect the crystal lattice to be promptly displaced along the superposition of the coordinates of these Raman modes.

Figure 9a depicts the time-resolved intensity changes of two selected diffraction peaks, which were measured at 100 K temperature using 50 fs X-ray pulses at 6.7 keV photon energy. Following the resonant excitation of the B_{1u} phonon mode with a fluence of 4 mJ/cm^2, we observed an increase and decrease of the (2 $\bar{1}$1) and the ($\bar{2}$ 0 4) peaks, respectively, both recovering

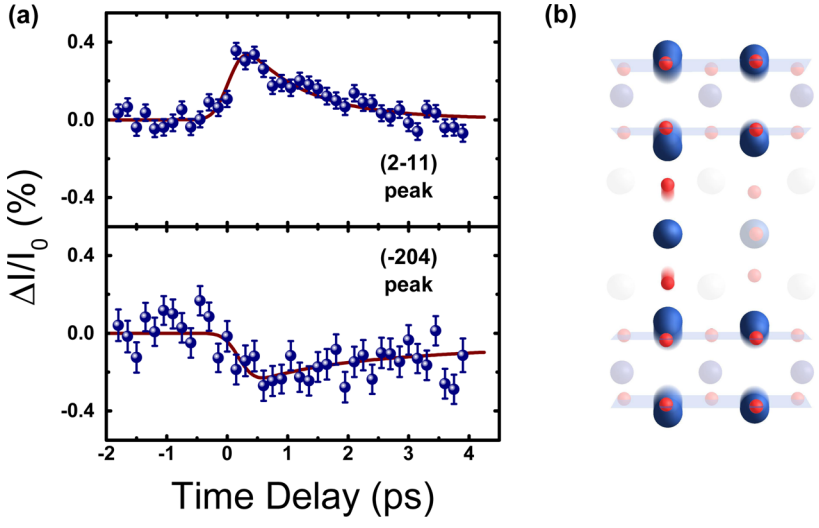

Figure 9. (a) Transient change in intensity of the (2 $\bar{1}$1) and the ($\bar{2}$ 0 4) diffraction peaks in $YBa_2Cu_3O_{6.5}$, measured at 100 K following resonant excitation of the B_{1u}-symmetry apical oxygen mode. The red solid lines are fits as described in the text. (b) Corresponding transient crystal structure of $YBa_2Cu_3O_{6.5}$. The atomic displacements from the equilibrium structure are shaded.

DOI: 10.1021/ar500391x
Acc. Chem. Res. 2015, 48, 380−387

to the equilibrium within the lifetime of the transient state measured in the terahertz probe experiments.[40,41] This similarity indicates a direct connection between the transient crystal structure and the light-induced coherent interlayer transport. The detailed atomic motions were determined by fitting these data, thereby considering the time-resolved measurement of further diffraction peaks, the computed coupling strength of the driven infrared-active mode to the A_g Raman phonons, and structure factor calculations of the involved Bragg diffraction peaks (see ref 43 for details of this procedure). Importantly, the intensity changes of all the measured peaks could be fitted simultaneously with the amplitude of the optically excited B_{1u} phonon being the only fitting parameter determining the sign and size in intensity change of all diffraction peaks. The results of these fits are shown as the red solid lines in Figure 9a.

A sketch of the corresponding transient crystal structure is shown in Figure 9b. The most apparent features of this lattice displacement are (i) the decrease of the distance between the apical oxygen and the copper atoms, (ii) the increase of the in-plane O−Cu−O buckling, (iii) the increase of the intrabilayer distance, and (iv) the decrease of the interbilayer distance. Particularly the latter two observations could intuitively describe the changes in coherent transport along the *c* axis. The decrease in interbilayer distance is expected to increase the tunneling between bilayers deduced from the measurement shown in Figure 8b. Furthermore, the increase in intrabilayer distance supports the recent experiments by Hu et al.,[40] who observed that this interbilayer tunneling is enhanced at the expense of coherent intrabilayer coupling.

■ CONCLUSION

Intense mid-infrared light fields can be used to drive solids into transient crystal structures not achievable at equilibrium. The coupling between different vibrational modes is key to this effect, which was demonstrated for third-order anharmonic coupling. In complex oxides, these lattice distortions can lead to electronic and magnetic phase changes, including insulator−metal transitions, rearrangements of spin and orbital order, and even enhanced superconductivity. In this Account, we have summarized the basic theoretical concept of and the recent achievements in this field, covering vibrationally induced phase transitions in manganites and the enhancement of superconductivity in cuprates. Ultrafast X-ray crystallography at free electron lasers provides knowledge of the nonequilibrium atomic structures that induce these exotic electronic properties. This insight might aid controlling the future of matter, which requires design rules for the development of materials exhibiting these exotic behaviors also at equilibrium.

■ AUTHOR INFORMATION

Corresponding Authors

*E-mail: michael.foerst@mpsd.mpg.de.
*E-mail: andrea.cavalleri@mpsd.mpg.de.

Author Contributions

The manuscript was written through contributions of all authors. All authors have given approval to the final version of the manuscript.

Notes

The authors declare no competing financial interest.

Biographies

Michael Först received his Ph.D. for his work on coherent carrier and lattice dynamics in semiconductors from the RWTH Aachen University in 2001. Currently, he is senior staff scientist at the Max-Planck Institute for the Structure and Dynamics of Matter with his research focusing on optical and X-ray probing of ultrafast lattice-driven phase transitions in strongly correlated electron systems.

Roman Mankowsky received his Diploma degree from the Humboldt University in Berlin. He is currently a Ph.D. candidate at the University of Hamburg and at the Max-Planck Institute for the Structure and Dynamics of Matter. His research involves the study of nonlinear lattice dynamics, with a focus on high-T_C cuprates.

Andrea Cavalleri received his Ph.D. from the University of Pavia, Italy, in 1998. He held research positions at the University of Essen (Germany), at the University of California, San Diego, and at the Lawrence Berkeley National Laboratory. In 2005, he joined the faculty of the University of Oxford, where he was promoted to Professor of Physics in 2006. Andrea Cavalleri became a Professor of Physics at the University of Hamburg in 2008 and is also the founding director of the Max Planck Institute for the Structure and Dynamics of Matter in Hamburg. Cavalleri has co-developed the field of ultrafast X-ray science and has been a pioneer in the optical of control emergent phases in quantum condensed matter.

■ ACKNOWLEDGMENTS

The authors thank R. Merlin, A. Subedi, and A. Georges for discussions and their contributions to this research field.

■ REFERENCES

(1) Khomskii, D. I. *Transition Metal Compounds*; Cambridge University Press: Cambridge, U.K., 2014.
(2) Kohler, B.; Krause, J. L.; Raksi, F.; Wilson, K. R.; Yakovlev, V. Y.; Whitnell, R. M.; Yan, Y. Controlling the Future of Matter. *Acc. Chem. Res.* **1995**, *28*, 133−140.
(3) Rabitz, H.; de Vivie-Riedle, R.; Motzkus, M.; Kompa, K. Whither the Future of Controlling Quantum Phenomena? *Science* **2000**, *288*, 824−828.
(4) Reddy, K. V.; Bray, R. G.; Berry, M. J. Dye Laser-Induced Photochemistry. In *Advances in Laser Chemistry*; Zewail, A. H., Ed.; Springer Verlag: Berlin, 1978.
(5) Nibbering, E. T. J.; Fidder, H.; Pines, E. Ultrafast Chemistry: Using Time-Resolved Vibrational Spectroscopy for Interrogation of Structural Dynamics. *Annu. Rev. Chem.* **2005**, *56*, 337−367.
(6) Wallis, R. F.; Maradudin, A. A. Ionic Raman Effect II: The First-Order Ionic Raman Effect. *Phys. Rev. B* **1971**, *3*, 2063−2075.
(7) Martin, T. P.; Genzel, L. Ionic Raman Scattering and Ionic Frequency Mixing. *Phys. Status Solidi B* **1974**, *61*, 493−502.
(8) Mills, D. L. Ionic Contribution to the Raman Tensor of Insulators. *Phys. Rev. B* **1987**, *35*, 9278−9283.
(9) Dhar, L.; Rogers, J.; Nelson, K. A. Time-Resolved Vibrational Spectroscopy in the Impulsive Limit. *Chem. Rev.* **1994**, *94*, 157−193.
(10) Merlin, R. Generating Coherent THz Phonons with Light Pulses. *Solid State Commun.* **1997**, *102*, 207−220.
(11) Stevens, T. E.; Kuhl, J.; Merlin, R. Coherent Phonon Generation and the Two Stimulated Raman Tensors. *Phys. Rev. B* **2002**, *65*, No. 144304.
(12) Okimoto, Y.; Katsufuji, T.; Ishikawa, T.; Arima, T.; Tomioka, Y.; Tokura, Y. Variation of Electronic Structure in $La_{1-x}Sr_xMnO_3$ ($0 \leqslant x \leqslant 0.3$) as Investigated by Optical Conductivity Spectra. *Phys. Rev. B* **1997**, *55*, 4206−4214.
(13) Först, M.; Manzoni, C.; Kaiser, S.; Tomioka, Y.; Tokura, Y.; Merlin, R.; Cavalleri, A. Nonlinear Phononics As an Ultrafast Route to Lattice Control. *Nat. Phys.* **2011**, *7*, 854−856.

DOI: 10.1021/ar500391x
Acc. Chem. Res. 2015, 48, 380−387

(14) Först, M.; Dekorsy, T. Coherent phonons in bulk and low-dimensional semiconductors. In *Coherent Vibrational Dynamics*; De Silvestri, S., Cerullo, G., Lanzani, G., Ed.; CRC Press: Boca Raton, FL, 2007, and references therein.
(15) Först, M.; Mankowsky, R.; Bromberger, H.; Fritz, D. M.; Lemke, H.; Zhu, D.; Chollet, M.; Tomioka, Y.; Tokura, Y.; Merlin, R.; Hill, J. P.; Johnson, S. L.; Cavalleri, A. Displacive Lattice Excitation through Nonlinear Phononics Viewed by Femtosecond X-ray Diffraction. *Solid State Commun.* **2013**, *169*, 24−27.
(16) Warren, B. E. *X-ray Diffraction*; Dover Publications: New York, 2009.
(17) Sokolowski-Tinten, K.; Blome, C.; Blums, J.; Cavalleri, A.; Dietrich, C.; Tarasevitch, A.; Uschmann, I.; Förster, E.; Kammler, M.; von Hoengen, M. H.; von der Linde, D. Femtosecond X-ray Measurement of Coherent Lattice Vibrations near the Lindemann Stability Limit. *Nature* **2003**, *422*, 287−289.
(18) Abrashev, M. V.; Litvinchuk, A. P.; Iliev, M. N.; Meng, R. L.; Popov, V. N.; Ivanov, V. G.; Chalakov, R. A.; Thomsen, C. Comparative Study of Optical Phonons in the Rhombohedrally Distorted Perovskites $LaAlO_3$ and $LaMnO_3$. *Phys. Rev. B* **1999**, *59*, 4146−4153.
(19) Granado, E.; Moreno, N. O.; Garcia, V.; Sanjurjo, J. A.; Rettori, C.; Torriani, V.; Oseroff, S. B.; Neumeier, J. J.; McClellan, K. J.; Cheong, S.-W.; Tokura, Y. Phonon Raman Scattering in $R_{1-x}A_xMnO_{3+\delta}$ (R=La, Pr; A=Ca, Sr). *Phys. Rev. B* **1998**, *58*, 11435−11440.
(20) Emma, P.; Akre, R.; Arthur, J.; Bionta, R.; Bostedt, C.; Bozek, J.; Brachmann, A.; Bucksbaum, P.; Coffee, R.; Decker, F.-J.; Ding, Y.; Dowell, D.; Edstrom, S.; Fisher, A.; Frisch, J.; Gilevich, S.; Hastings, J.; Hays, G.; Hering, Ph.; Huang, Z.; Iverson, R.; Loos, H.; Messerschmidt, M.; Miahnahri, A.; Moeller, S.; Nuhn, H.-D.; Pile, G.; Ratner, D.; Rzepiela, J.; Schultz, D.; Smith, T.; Stefan, P.; Tompkins, H.; Turner, J.; Welch, J.; White, W.; Wu, J.; Yocky, G.; Galayda, J. First Lasing and Operation of an Ångstrom-Wavelength Free-Electron Laser. *Nat. Photonics* **2010**, *4*, 641−647.
(21) Goodenough, J. B. Theory of the Role of Covalence in the Perovskite-Type Manganites [La, M(II)]MnO_3. *Phys. Rev.* **1955**, *100*, 564−573.
(22) Tomioka, Y.; Asamitsu, A.; Kuwahara, H.; Moritomo, Y. Magnetic-Field-Induced Metal-Insulator Phenomena in $Pr_{1-x}Ca_xMnO_3$ with Controlled Charge-Ordering Instability. *Phys. Rev. B* **1996**, *53*, 1689−1692.
(23) Asamitsu, A.; Tomioka, Y.; Kuwahara, H.; Tokura, Y. Current Switching of Resistive States in Magnetoresistive Manganites. *Nature* **1997**, *388*, 50−52.
(24) Kiriukhin, V.; Casa, D.; Hill, J. P.; Keimer, B.; Vigliante, A.; Tomioka, Y.; Tokura, Y. An X-ray-Induced Insulator−Metal Transition in a Magnetoresistive Manganite. *Nature* **1997**, *386*, 813−815.
(25) Miyano, K.; Tanaka, T.; Tomioka, Y.; Tokura, Y. Photoinduced Insulator-to-Metal Transition in a Perovskite Manganite. *Phys. Rev. Lett.* **1997**, *78*, 4257−4260.
(26) Fiebig, M.; Miyano, K.; Tomioka, Y.; Tokura, Y. Visualization of the Local Insulator-Metal Transition in $Pr_{0.7}Ca_{0.3}MnO_3$. *Science* **1998**, *280*, 1925−1928.
(27) Hwang, H. Y.; Palstra, T. T. M.; Cheong, S.-W.; Batlogg, B. Pressure Effects on the Magnetoresistance in Doped Manganese Perovskites. *Phys. Rev. B* **1995**, *52*, 15046−15049.
(28) Rini, M.; Tobey, R.; Dean, N.; Itatani, J.; Tomiaka, Y.; Tokura, Y.; Schoenlein, R. W.; Cavalleri, A. Control of the Electronic Phase of a Manganite by Mode-Selective Vibrational Excitation. *Nature* **2007**, *449*, 72−74.
(29) Subedi, A.; Cavalleri, A.; Georges, A. Theory of Nonlinear Phononics for Coherent Light Control of Solids. *Phys. Rev. B* **2014**, *89*, No. 220301.
(30) Sternlieb, B. J.; Hill, J. P.; Wildgruber, U. C.; Luke, G. M.; Nachumi, B.; Moritomo, Y.; Tokura, Y. Charge and Magnetic Order in $La_{0.5}Sr_{1.5}MnO_4$. *Phys. Rev. Lett.* **1996**, *76*, 2169−2172.
(31) Tobey, R. I.; Prabhakaran, D.; Boothroyd, A. T.; Cavalleri, A. Ultrafast Electronic Phase Transition in $La_{1/2}Sr_{3/2}MnO_4$ by Coherent Vibrational Excitation: Evidence for Non-thermal Melting of Orbital Order. *Phys. Rev. Lett.* **2008**, *101*, No. 197404.
(32) Först, M.; Tobey, R.; Wall, S.; Bromberger, H.; Khanna, V.; Cavalieri, A.; Chuang, Y.-D.; Lee, W. S.; Moore, R.; Schlotter, W.; Turner, J.; Krupin, O.; Trigo, M.; Zheng, H.; Mitchell, J.; Dhesi, S.; Hill, J.; Cavalleri, A. Driving Magnetic Order in a Manganite by Ultrafast Lattice Excitation. *Phys. Rev. B* **2011**, *84*, No. 241104.
(33) Beaud, P.; Johnson, S. L.; Vorobeva, E.; Staub, U.; De Souza, R. A.; Milne, C. J.; Jia, Q. X.; Ingold, G. Ultrafast Structural Phase Transition Driven by Photoinduced Melting of Charge and Orbital Order. *Phys. Rev. Lett.* **2009**, *103*, No. 155702.
(34) Ehrke, H.; Tobey, R. I.; Wall, S.; Cavill, S. A.; Först, M.; Khanna, V.; Garl, Th.; Stojanovic, N.; Prabhakaran, D.; Boothroyd, A. T.; Gensch, M.; Mirone, A.; Reutler, P.; Revcolevschi, A.; Dhesi, S. S.; Cavalleri, A. Photoinduced Melting of Antiferromagnetic Order in $La_{0.5}Sr_{1.5}MnO_4$ Measured Using Ultrafast Resonant Soft X-ray Diffraction. *Phys. Rev. Lett.* **2011**, *106*, No. 217401.
(35) Singla, R.; Simoncig, A.; Först, M.; Prabhakaran, D.; Cavalieri, A. L.; Cavalleri, A. Photoinduced Melting of the Orbital Order in $La_{0.5}Sr_{1.5}MnO_4$ with 4-fs Laser Pulses. *Phys. Rev. B* **2013**, *88*, No. 075107.
(36) Beaud, P.; Caviezel, A.; Mariager, S. O.; Rettig, L.; Ingold, G.; Dornes, C.; Huang, S.-W.; Johnson, J. A.; Radovic, M.; Huber, T.; Kubacka, T.; Ferrer, A.; Lemke, H. T.; Chollet, M.; Zhu, D.; Glownia, J. M.; Sikorski, M.; Robert, A.; Wadati, H.; Nakamura, M.; Kawasaki, M.; Tokura, Y.; Johnson, S. L.; Staub, U. A Time-Dependent Order Parameter for Ultrafast Photoinduced Phase Transitions. *Nat. Mater.* **2014**, *13*, 923−927.
(37) Caviglia, A. D.; Scherwitzl, R.; Popovich, P.; Hu, W.; Bromberger, H.; Singla, R.; Mitrano, M.; Hoffmann, M. C.; Kaiser, S.; Zubko, P.; Gariglio, S.; Triscone, J. M.; Först, M.; Cavalleri, A. Ultrafast Strain Engineering in Complex Oxide Heterostructures. *Phys. Rev. Lett.* **2012**, *108*, No. 136801.
(38) Fausti, D.; Tobey, R. I.; Dean, N.; Kaiser, S.; Dienst, A.; Hoffmann, M. C.; Pyon, S.; Takayama, T.; Takagi, H.; Cavalleri, A. Light-Induced Superconductivity in a Stripe-Ordered Cuprate. *Science* **2011**, *331*, 189−191.
(39) Först, M.; Tobey, R. I.; Bromberger, H.; Wilkins, S. B.; Khanna, V.; Caviglia, A. D.; Chuang, Y.-D.; Lee, W. S.; Schlotter, W. F.; Turner, J. J.; Minitti, M. P.; Krupin, O.; Xu, Z. J.; Wen, J. S.; Gu, G. D.; Dhesi, S. S.; Cavalleri, A.; Hill, J. P. Melting of Charge Stripes in Vibrationally Driven $La_{1.875}Ba_{0.125}CuO_4$: Assessing the Respective Roles of Electronic and Lattice Order in Frustrated Superconductors. *Phys. Rev. Lett.* **2014**, *112*, No. 157002.
(40) Hu, W.; Kaiser, S.; Nicoletti, D.; Hunt, C. R.; Gierz, I.; Hoffmann, M. C.; Le Tacon, M.; Loew, T.; Keimer, B.; Cavalleri, A. Optically Enhanced Coherent Transport in $YBa_2Cu_3O_{6.5}$ by Ultrafast Redistribution of Interlayer Coupling. *Nat. Mater.* **2013**, *13*, 705−711.
(41) Kaiser, S.; Hunt, C. R.; Nicoletti, D.; Hu, W.; Gierz, I.; Liu, H. Y.; Le Tacon, M.; Loew, T.; Haug, D.; Keimer, B.; Cavalleri, A. Optically Induced Coherent Transport Far above Tc in Underdoped $YBa_2Cu_3O_{6+x}$. *Phys. Rev. B* **2014**, *89*, No. 184516.
(42) Anderson, P. W. Interlayer Tunneling Mechanism for High-TC Superconductivity: Comparison with c Axis Infrared Experiments. *Science* **1995**, *268*, 1154−1155.
(43) Mankowsky, R.; Subedi, A.; Först, M.; Mariager, S. O.; Chollet, M.; Lemke, H. T.; Robinson, J. S.; Glownia, J. M.; Minitti, M. P.; Frano, A.; Fechner, M.; Spaldin, N. A.; Loew, T.; Keimer, B.; Georges, A.; Cavalleri, A. Nonlinear Lattice Dynamics As a Basis for Enhanced Superconductivity in $YBa_2Cu_3O_{6.5}$. *Nature* **2014**, *516*, 71−73.

DOI: 10.1021/ar500391x
Acc. Chem. Res. 2015, 48, 380−387